Available online at www.sciencedirect.com

ScienceDirect

Advances in Space Research 68 (2021) 4932–4947

ADVANCES IN SPACE RESEARCH (a COSPAR publication)

www.elsevier.com/locate/asr

Multi-frequency multi-GNSS receiver antenna calibration at IfE: Concept - calibration results - validation

Johannes Kröger *, Tobias Kersten, Yannick Breva, Steffen Schön

Leibniz Universität Hannover, Institut für Erdmessung (IfE), Schneiderberg 50, D-30167 Hannover, Germany

Received 31 January 2020; received in revised form 5 January 2021; accepted 17 January 2021
Available online 28 January 2021

Abstract

Multi-frequency and multi-constellation GNSS have the potential to boost the overall performance of GNSS-based positioning, navigation and timing. This has an impact on the realisation of global reference frames, geophysical monitoring applications as well as enabling new applications. To this end, all error sources should be adequately corrected for. However, currently multi-frequency multi-GNSS receiver antenna calibration values are still missing. In this paper, the newly developed multi-frequency multi-GNSS calibration process at Institut für Erdmessung (IfE), Leibniz University Hannover, is presented. The basic concept and the assumptions for the antenna calibration are described. Resulting phase centre corrections (PCC) for GPS and Galileo for typical antennas are presented. We show that the repeatability of the estimated patterns are almost better than 2 mm in terms of maximum deviation and that the used tracking strategies by the receivers have marginal impact on the patterns, at maximum 1.2 mm for the studied receiver-antenna combinations. Furthermore, applying phase centre corrections for multi-frequency multi-GNSS carrier phase observations reduces significantly (up to 37%) the antenna related biases as validated on short baselines. Moreover, a validation in the coordinate domain shows that with IfE PCC a short baseline can be computed with high accuracy: the topocentric coordinate differences to the known baseline are in most cases smaller than 1 mm for the horizontal components and smaller than 2.2 mm in vertical.

Keywords: GNSS receiver antennas; Phase centre corrections; Absolute antenna calibration; Multi-GNSS

1. Introduction

Global Navigation Satellite Systems (GNSS) enable not only positioning, navigation and timing (PNT) but also contribute to the realisation and densification of geodetic reference frames (Altamimi et al., 2016) and allow highly accurate monitoring from landslides (Schön, 2007) to plate tectonics (Kreemer et al., 2014; DeMets et al., 2010). Four GNSS are recently available: the US-American Global Positioning System (GPS), the European Galileo, the Russian GLONASS and the Chinese Beidou System. Regional overlay systems like the Indian regional Navigation satellite system (IRNSS) or the Japanese Quasi Zenith satellite system (QZSS) as well as the Wide Area Augmentation System (WAAS) or European geostationary navigation overlay service (EGNOS) augment the GNSS.

One of the most challenging issues for using all GNSS for positioning and timing is the lack of consistent multi-frequency multi-GNSS phase centre corrections (PCC) for the user segment. The official International GNSS Service (IGS, (Johnston et al., 2017)) Antenna Exchange (ANTEX, (Rothacher and Schmid, 2010)) file (igs14.atx, in its current version igs14_2086.atx) contains dual-frequency PCC for GPS and GLONASS for receiver antennas only. The majority of entries in the IGS ANTEX file are type mean values and they are determined by the

* Corresponding author.
E-mail address: kroeger@ife.uni-hannover.de (J. Kröger).
URL: http://www.ife.uni-hannover.de (J. Kröger).

https://doi.org/10.1016/j.asr.2021.01.029
0273-1177/

method ROBOT, based on the concept of absolute field calibration described in Menge et al. (1998),Wübbena et al. (2000), Böder et al. (2001). This approach was developed in Hannover in close cooperation between the Institut für Erdmessung (IfE) and Geo++.

For ground station antennas, multi-GNSS PCC can be determined by chamber calibration (Görres et al., 2006; Becker et al., 2010; Zeimetz, 2010). Some of these individual calibrations are available for 34 antennas in the European Permanent Network (EPN) (Bruyninx and Legrand, 2017). The potential of using such fully calibrated multi-GNSS antennas for reference frame applications has been demonstrated by Villiger et al. (2018),Villiger et al. (2019) at different conferences. Schmolke et al. (2015) reported first field based multi-frequency multi-GNSS PCC obtained by the relative antenna calibration approach.

At present, several groups are working on developing and updating their approaches and facilities for absolute PCC determination, underlining the importance of the topic *antenna calibration* for geodesy. Geo++ recently presented first multi-frequency multi-GNSS calibration results (Wübbena et al., 2019). The U.S. National Geodetic Survey (NGS) is developing their 2-axis robot (Mader et al., 2012) to a 6-axis robot system (Bilich et al., 2018). The ETH Zurich recently presented their system based on a 6-axis robot (Willi et al., 2019). In addition, further research is ongoing at Wuhan University China (Hu et al., 2015) and at University at Warmia, Poland. These activities underline the essential need to provide multi-GNSS PCC for receiver ground stations and network operators.

In order to close the gap of available multi-GNSS PCC determined by the ROBOT method, our group at IfE investigated an independent approach for processing and estimating PCC for new signals based on time differenced single differences (Kersten and Schön, 2010; Kersten, 2014; Kröger et al., 2019). This concept is different to the undifferenced approach presented by Wübbena et al. (2019). Nevertheless, the same 5-axis robotic system is used in both methods to accurately rotate and tilt the antenna under test (AUT) w.r.t. the current satellite constellation.

This paper is structured as follows: In Section 2, the theoretical background of PCC is explained. Next, in Section 3 the calibration method used at IfE is presented. This contains mainly three parts: the data acquisition, the preprocessing of GNSS data and finally the estimation of the PCC. Results of obtained PCC for different types of antennas that are widely used in the IGS network are shown in Section 4 including the analysis of repeatability of different calibrations (Section 5.1) as well as the repeatability with different receivers (Section 5.2). Consequently, in Section 6 the validation of the PCC in the observation and coordinate domain is presented. Section 7 closes the paper with conclusion.

2. Theoretical background

The quality and reception properties of the GNSS receiving antenna depend on various parameters (Stutzman, 2013) including on the one hand, the individual design parameters (gain, multipath reduction, stable PCC, low-loss data transmission with an optimum voltage standing wave ratio (VSWR), optimum impedance, ground plane, etc.). On the other hand, its response to reflecting and conducting materials in the vicinity has to be considered. Therefore, various compromises have to be made during the design and production process of GNSS receiver antennas (Rao et al., 2013). As a consequence, the electric phase centre, which represents the location where the actual measurement takes place, is changing with the direction of the satellite signal and differs from an ideal omni-directional pattern.

In order to obtain ultimate quality for GNSS positioning, adequate corrections (known as PCC) must be applied. Traditionally, the PCC is arbitrarily subdivided into the phase centre offset (PCO) projected on the line-of-sight $\vec{e}(\alpha^k, z^k)$, and the azimuth α and zenith angle z dependent phase centre variations (PCV). Due to the relative character of GNSS observations (i.e. pseudo-ranges), a constant part r is also present, which is linked to the receiver clock in case of field calibrations or to the ambiguities in the network analyzer in case of chamber calibrations. This constant parameter cannot be resolved without additional information.

$$PCC(\alpha^k, z^k) = -PCO \cdot \vec{e}(\alpha^k, z^k) + PCV(\alpha^k, z^k) + r \tag{1}$$

In order to provide a unique solution, a datum has to be defined to remove the rank deficiency of the analysis set-up. This is typically done either by constraining the corrections at zenith to zero (zero zenith constraint) or by a zero mean constraint over the whole or a part of the antenna hemisphere (Rothacher et al., 1995).

Following the conventions of the IGS, the PCC are expressed in an antenna fixed left-handed coordinate system, where the positive z-axis points into the antenna bore-sight direction and the x-axis in the direction of the antenna's north mark, which is mostly the antenna cable connector. The origin of the coordinate system is located at the antenna reference point (ARP), which is situated at a mechanically accessible point, usually the substructure of the antenna. Fig. 1 shows the geometrical interpretation of the PCC in a sketch, where $\vec{e}$ indicates the line-of-sight (LOS) unit vector towards a specific satellite k.

The GPS and GLONASS L1 and L2 PCC are provided in the ANTEX format by the IGS and its antenna working group. The PCV are tabulated as a grid with a typical resolution of 5° azimuth and 5° zenith steps from 0° to 360° in azimuth and 0° to 90° in zenith direction. Along with it, the

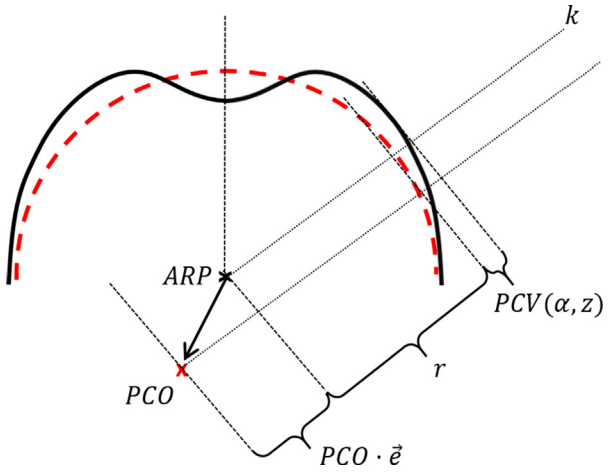

Fig. 1. Sketch of the geometrical interpretation of the PCC. The red dashed line indicates the theoretical onmi-directional radiation pattern of a GNSS receiver antenna while the solid line represents the real pattern. Differences between ideal and real phase front are defined as PCC. (For interpretation of the references to color in this figure legend, the reader is referred to the web version of this article.)

PCO is published as a 3D offset vector of the mean phase centre location with respect to the ARP (Rothacher and Schmid, 2010).

When different sets of PCC of the same antenna (e.g. PCC_1, PCC_2) are compared, it is important to take (i) differences in PCO and (ii) different datum definitions correctly into account. The best is to compare only the total PCC since they contain all information. If PCV are of interest, for (i) a transformation has to be done

$$PCV_{1,2}(\alpha, z) = (PCO_2 - PCO_1) \cdot \vec{e}(\alpha, z) + PCV_1(\alpha, z) + \Delta r \quad (2)$$

to relate the different PCC to a common PCO set (Menge et al., 1998); here shown as an example for PCC_1, assuming that PCO_2 is the common PCO. After transformation on PCO_2, $PCV_{1,2}$ can be compared to PCV_2

Since the datum definition of each calibration facility is generally not reported, a datum transformation as known in other geodetic context, like e.g. geodetic networks, cannot be applied. Subsequently, Schön and Kersten (2013) proposed different comparison strategies. Especially the datum independent spread ($s = PCC_{max} - PCC_{min}$) should be chosen to compare different sets of PCC by $\Delta s = (PCC_{1_{max}} - PCC_{1_{min}}) - (PCC_{2_{max}} - PCC_{2_{min}})$.

3. Methodology of calibration

3.1. Data acquisition

In order to estimate absolute PCC in the field, IfE uses a circa one meter high industrial robot with 5 degrees of freedom. It can precisely rotate and tilt the AUT in short time intervals ($\Delta \approx 1\,s$) around a fixed point in space with a repositioning accuracy of about 0.25 mm (Kersten, 2014).

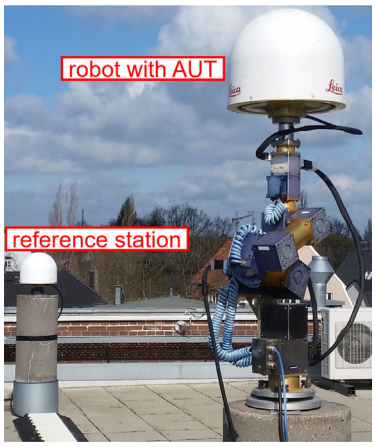

Fig. 2. Calibration set-up at IfE. In the front the robot with the AUT (in this case LEIAR25.R3) can be seen. At a distance of about 8 m the reference station is located.

At a distance of approximately 8 m, a geodetic reference antenna is set up (LEIAR25.R3 LEIT) as shown in Fig. 2. Both antennas are connected to the same type of receiver. An external frequency standard (Standard Rubidium FS725) with a stability of $< 2 \cdot 10^{-11}$ is linked to the receivers, so that the individual receiver clock drift is identical at both receivers (Kersten, 2014). Predefined sequences of movements for the robot position are used that are slightly adapted to the GPS satellite geometry, i.e. the actually visible satellites.

During the calibration, which takes about 4 h depending especially on the weight and height of the AUT, the GNSS raw data of both receivers as well as the movements of the robot with the corresponding timestamps are logged. With these orientation parameters and the observations, the data can be processed in a post-processing approach for the PCC estimation.

3.2. Data preprocessing

First, the common timestamps are compared between the GNSS raw data and the robot poses when the robot is not moving. Subsequently, the actual position of the AUT is calculated using the robot calibration values for the arm lengths and the remaining offsets between the robot modules determined by the laser tracker (Kersten, 2014, p. 56 ff). Afterwards, the azimuth and elevation angle of the satellite is transformed into the antenna frame. Finally, time-differenced receiver-to-receiver single differences (dSD) are computed, so that most of the GNSS error budget, such as signal propagation errors by ionospheric or tropospheric refraction, orbit errors and common parts of the receiver clock errors are cancelled on the 8 m baseline.

Thanks to these time differences, the ambiguity term is removed as well as the impact of the PCC of the second antenna at the reference station. Furthermore, due to the short time intervals between subsequent epochs multipath effects are strongly reduced since the station's surroundings

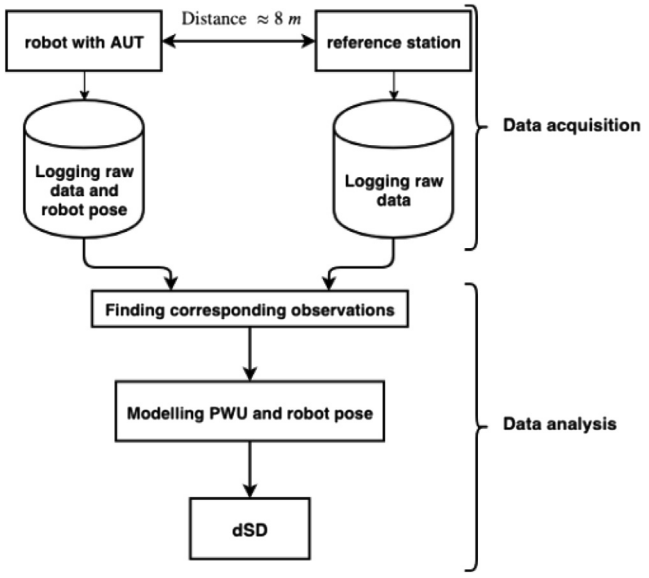

Fig. 3. Process chain of the data acquisition and analysis at IfE. The resulting dSD are used afterwards for the PCC estimation.

do not change. The phase-wind up (PWU) effect (Wu et al., 1993) is modelled using the robot pose so that subsequently the corrected dSD only contain the PCC of the AUT plus noise ϵ

$$dSD^k = PCC^k_{AUT}(t_{i+1}) - PCC^k_{AUT}(t_i) + \epsilon(t_i, t_{i+1}). \quad (3)$$

Fig. 3 summarises the data acquisition and analysis.

3.3. PCC estimation

The PCC are typically parameterised by spherical harmonic (SH) functions using degree m = 8 and order n = 8. Eq. (4) shows the SH with $\tilde{P}$ denoting the fully normalised Legendre function, z and α the zenith and azimuth angle to satellite k in the antenna frame, and a_{mn} together with b_{mn} the unknowns which are estimated in a least-squares adjustment.

$$PCC(a^k, z^k) = \sum_{m=1}^{m_{max}} \sum_{n=0}^{m} \tilde{P}_{mn}(cosz^k) \cdot (a_{mn} cos(n\alpha^k) + b_{mn} sin(n\alpha^k)) \quad (4)$$

Eq. (5) gives the functional model for the least-squares adjustment. The design matrix $\boldsymbol{A}$ is filled with the partial derivatives of Eq. (4) with respect to the unknowns and **dSD** is the vector of dSD observations. In a first step, all observations are equally weighted.

$$\hat{\boldsymbol{x}} = \left(\boldsymbol{A}^T \boldsymbol{A}\right)^{-1} \cdot \boldsymbol{A}^T \boldsymbol{dSD} \quad (5)$$

The design matrix $\boldsymbol{A_k}$ is set up epoch-wise for each satellite k so that the normal equation matrix $\boldsymbol{N_k}$ for each satellite reads

$$\boldsymbol{N_k} = \boldsymbol{A_k^T}\, \boldsymbol{A_k} \quad (6)$$

and is then added up over all satellites

$$\bar{\boldsymbol{N}} = \sum_{k=1}^{k_{Max}} \boldsymbol{N_k}. \quad (7)$$

The stacking is performed equivalently for the right side of the normal equation system

$$\boldsymbol{n_k} = \boldsymbol{A_k^T dSD_k} \quad (8)$$

$$\bar{\boldsymbol{n}} = \sum_{k=1}^{k_{Max}} \boldsymbol{n_k}. \quad (9)$$

As only observations are present on the upper hemisphere of the antenna, the normal equation matrix $\bar{\boldsymbol{N}}$ is poorly conditioned. To improve the condition, coefficients a_{mn} and b_{mn} with an odd index sum (e.g. a_{21}, b_{21}, a_{30}) are restricted to zero since they express the anti-symmetry between the upper and lower half of the sphere:

$$\tilde{\boldsymbol{N}} = \begin{bmatrix} \bar{\boldsymbol{N}} & \boldsymbol{R}^T \\ \boldsymbol{R} & \boldsymbol{0} \end{bmatrix} \quad (10)$$

with $\boldsymbol{R}$ being the restriction matrix and

$$\tilde{\boldsymbol{n}} = \begin{bmatrix} \bar{\boldsymbol{n}} \\ \boldsymbol{0} \end{bmatrix} \quad (11)$$

for the right side. By inverting $\tilde{\boldsymbol{N}}$, the normal equation system is solved for the unknowns a_{mn} and b_{mn}

$$\hat{\boldsymbol{x}} = \tilde{\boldsymbol{N}}^{-1} \cdot \tilde{\boldsymbol{n}}. \quad (12)$$

Next, the grid values are obtained. To this end, the estimated unknowns are inserted into Eq. (4) with azimuth angles from 0° to 360°, zenith angles from 0° to 90° and a step size of 5°, respectively. Subsequently, the PCC grid is transformed into PCO and PCV. In this step, the zero zenith constraint is explicitly formulated. Finally, a constant PCO part and the corresponding PCV are written into the ANTEX format.

Currently, the individual frequencies are denoted as G01, G02 and R01, R02, respectively, in the ANTEX file. However, due to newer frequencies but especially due to different tracking algorithms of the receivers a transition of the frequencies specifications to the Receiver Independent Exchange Format (RINEX; IGS (2015),IGS (2015)) convention would not only be reasonable but also more consistent for the users, if significant differences are confirmed.

In addition, equivalently to PCC, antenna specific code phase corrections (CPC) – also known and used as group delay variations (GDV) – can be estimated for GNSS receiving antennas, see Wübbena et al. (2019),Kersten (2014) for robot calibration, Caizzone et al. (2019), Garbin et al. (2018) for chamber calibration for aviation and time transfer, respectively, and Wanninger et al. (2017) for a determination from a global network. The CPC reach orders of magnitudes of some dm that should

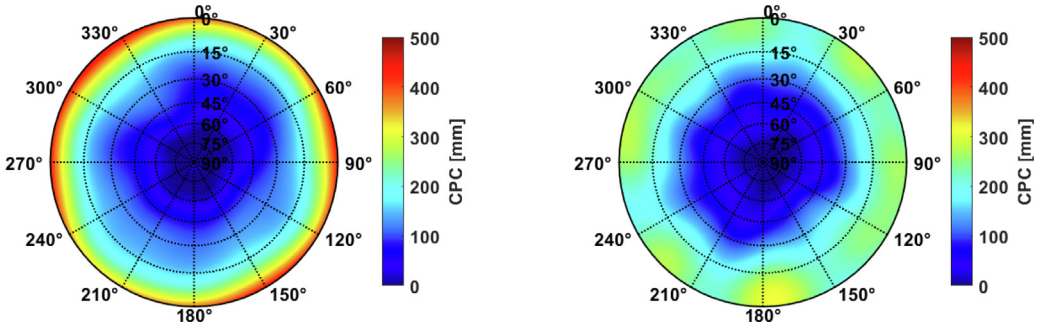

(a) GC1C (b) EC1X

Fig. 4. CPC for LEIAR25.R3 LEIT for GC1C and EC1X.

no longer be neglected (Beer et al., 2019; Kersten and Schön, 2017).

For instance, Fig. 4 shows CPC, which were estimated at IfE, for a LEIAR25.R3 LEIT antenna. It can be seen, that the GC1C corrections are in a range of up to 45 cm whereas the corrections for EC1X are smaller and reach a magnitude of approximately 30 cm (Breva et al., 2019).

Thus, future work is needed to focus on the additional integration of CPC into the ANTEX format. Table 1 demonstrates exemplarily for GPS and Galileo, how the frequency specification would change. As it can be seen from the table, for each frequency band and system currently one single specifier is defined in the ANTEX file, e.g. G01 for GPS frequency band L1. However, this specifier encompasses different tracking algorithm like GL1C and GL1X. Therefore, with this type of specifier it would not be possible to introduce CPC/GDV into the ANTEX file in a consistent way.

4. Estimated PCC

During February and August 2019 several calibrations of different antennas and antenna types have been carried out at IfE. Fig. 5 shows the resulting PCC (including PCO and PCV) for GPS and Galileo frequency band L1/E1 and L5/E5 for a LEIAR20 LEIM antenna.The gridded PCC are transformed into polar coordinates for a better representation. Here, the centre of the individual figure represents the zenith direction while the local antenna horizon is depicted at the border. For reasons of clarity of representation, the PCC are transformed by $PCC' = PCC - cos(z)\,PCO_{Up}$ so that the corrections are zero at zenith (i.e. the centre of the plot) and the up-component of the PCO is fully visible at the horizon. It can be seen, that the PCC reaches up to 15 cm. Moreover, the frequency dependency becomes clear since the PCC of GL1C and EL1X as well as GL5X and EL5X, respectively, have similar behaviour inside the bands, but show differences for the different frequency bands. Furthermore, only marginal variations in azimuth can be observed whereas larger elevation-dependent variations are present. Fig. 6 presents the estimated PCC for LEIAR25 LEIT. The PCC data for this antenna is provided on our institutional data repository (Kröger et al., 2019). The same behaviour of the PCC as in Fig. 5 can be observed: only marginal variations in azimuth are present. However, the PCC have a slightly higher magnitude at low elevations.

In Fig. 7 the calibration results for antenna NOV703GGG.R2 are shown. The PCC data is also available in ANTEX format for further investigations (Kröger et al., 2019). This is a smaller rover antenna (see Fig. 14, in the foreground) with a maximum PCC of circa 7 cm at low elevations. However, small variations in azimuth range can be observed especially for L5 at low elevations and for instance an azimuth angle between 180° and 270°.

Fig. 8 depicts the differences of PCC (Δ PCC) between similar frequencies of GPS and Galileo. Differences up to 3.91 mm at low elevations can be seen in Fig. 8(a) for L1, whereas the differences Δs of the datum independent spread is 1.67 mm. Similar behaviour is observed in

Table 1
Frequency specification corresponding to RINEX observation codes and their transition into ANTEX format, exemplarily shown for carrier phases.

GNSS System	ANTEX	Band	RINEX signal and channel specifier
GPS	G01	L1	GL1C, GL1S, GL1L, GL1X, GL1P, GL1W, GL1M, GL1N
	G02	L2	GL2C, GL2D, GL2S, GL2L, GL2X, GL2P, GL2W, GL2Y, GL2M, GL1N
	G05	L5	GL5I, GL5Q, GL5X
Galileo	E01	E1	EL1A, EL1B, EL1C, EL1X, EL1Z
	E05	E5a	EL5Q, EL5I, EL5X
	E07	E5b	EL7Q, EL7I, EL7X
	E08	E5ab	EL8Q, EL8I, EL8X
	E06	E6	EL6Q, EL6I, EL6X

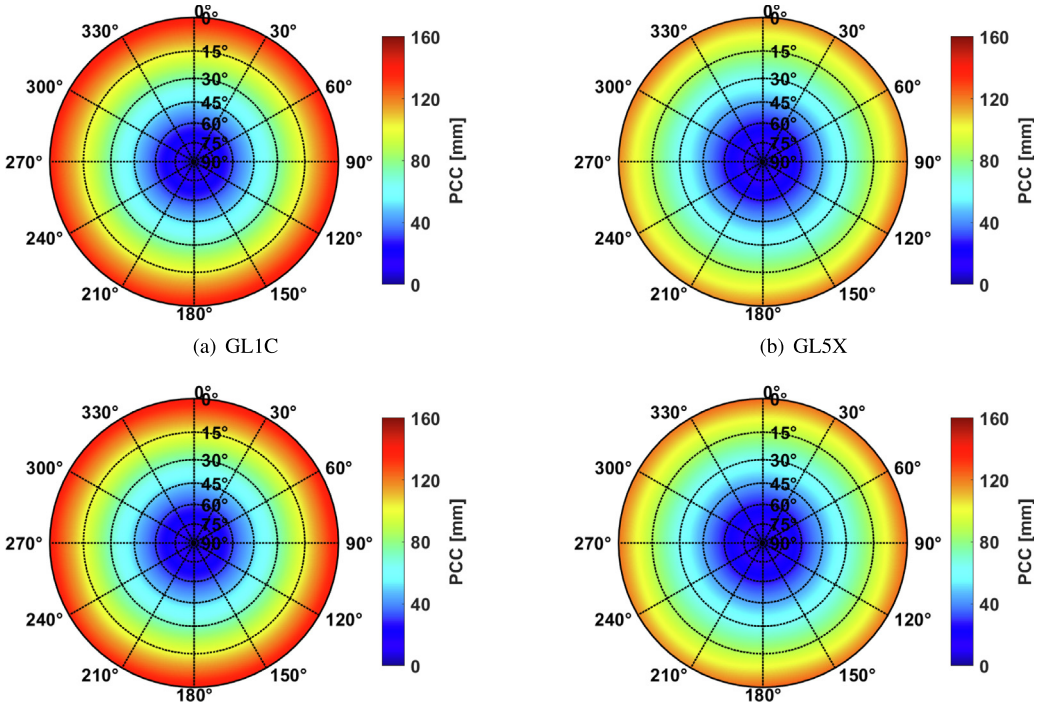

(a) GL1C (b) GL5X

(c) EL1X (d) EL5X

Fig. 5. PCC for LEIAR20 LEIM for GL1C, GL5X, EL1X and EL5X.

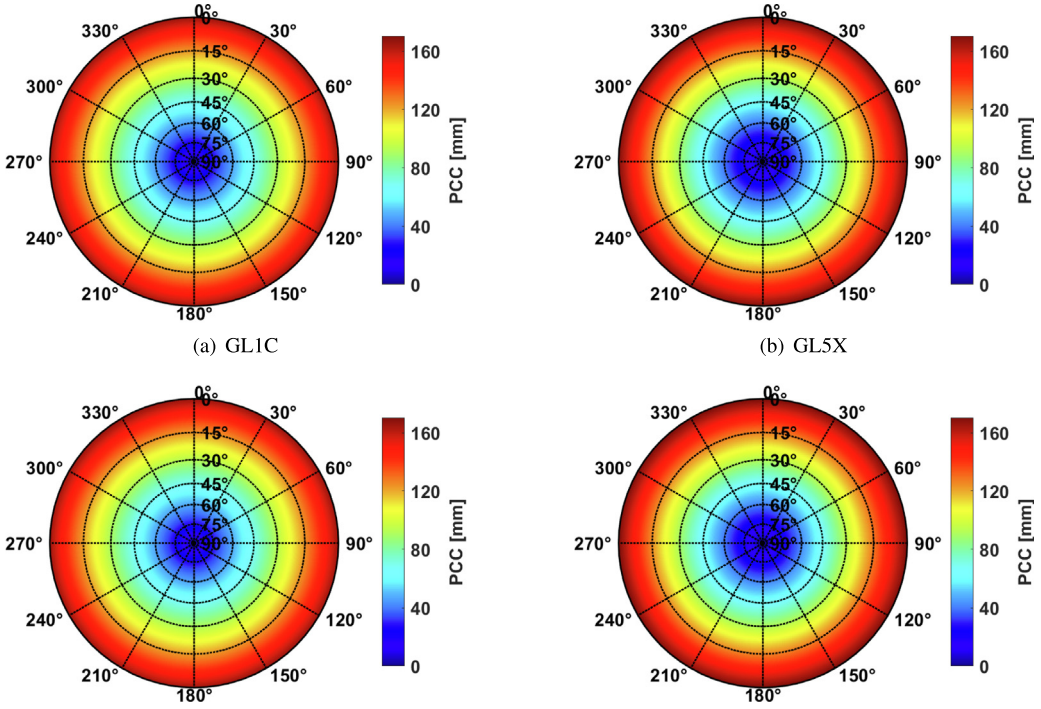

(a) GL1C (b) GL5X

(c) EL1X (d) EL5X

Fig. 6. PCC for LEIAR25.R3 LEIT for GL1C, GL5X, EL1X and EL5X.

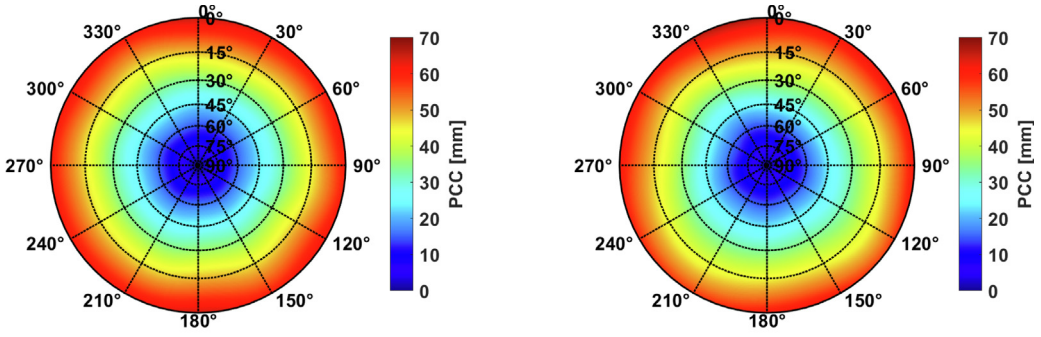

(a) GL1C (b) GL5X

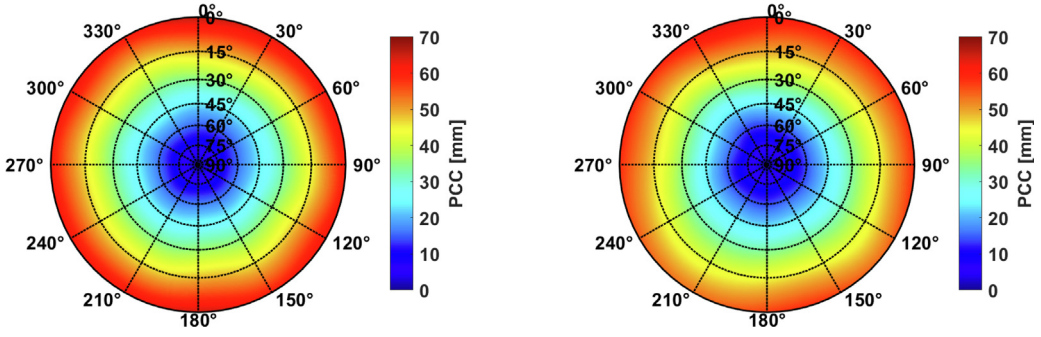

(c) EL1X (d) EL5X

Fig. 7. PCC for NOV703GGG.R2 NONE for GL1C, GL5X, EL1X and EL5X.

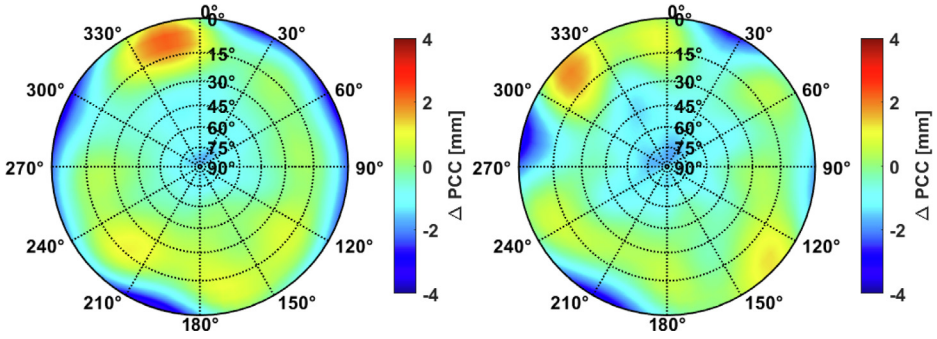

(a) Δ PCC (GL1C - EL1X) (b) Δ PCC (GL5X - EL5X)

Fig. 8. Δ PCC for LEIAR20 LEIM between similar frequencies of different GNSS.

Fig. 8(b) for L5. Here, the maximum difference is 3.28 mm and the spread 0.17 mm.

Comparable results are also obtained if the respective PCC are estimated with an approximately same number of GPS and Galileo observations per 5° elevation bin. The number per azimuth bin were not adapted since the observations are in this case more equally distributed. This suggests, that not only frequency specific but also system specific PCC should be provided. Since the Δ PCC is not restricted to zero, an offset in the up-component ΔPCO_U between the two GNSS is present at zenith. For L1/E1 it is 1.24 mm and for L5/E5 1.26 mm, respectively. However, the differences of the north and east component of the PCO are below 0.3 mm for L1 and smaller than 0.2 mm for L5.

5. Repeatability of estimated PCC

5.1. Repeatability of individual calibration

In order to assess the repeatability of the estimated PCC, multiple calibrations of the same antenna (LEIAR20 LEIM) were performed in August 2019. Fig. 9(a) shows the elevation-dependent Δ PCC between DOY224 and DOY225. The same receivers and receiver settings were used in these two different calibrations. As the robot operation was optimised for the current GPS satellite geometry, the robot poses are not exactly identical but quite comparable. Differences are less than 1 mm for GL1C, EL1X and EL5X. For GL5X, however, the differences are larger

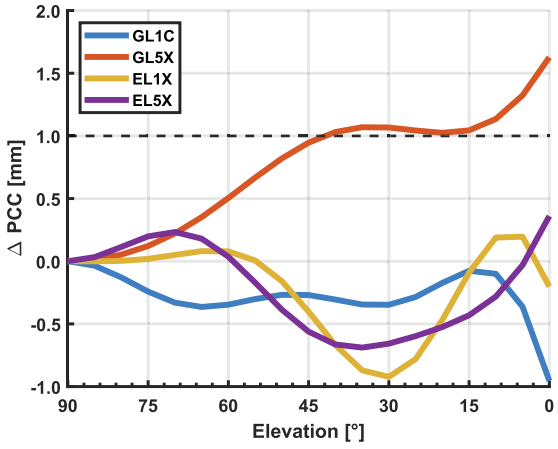

(a)

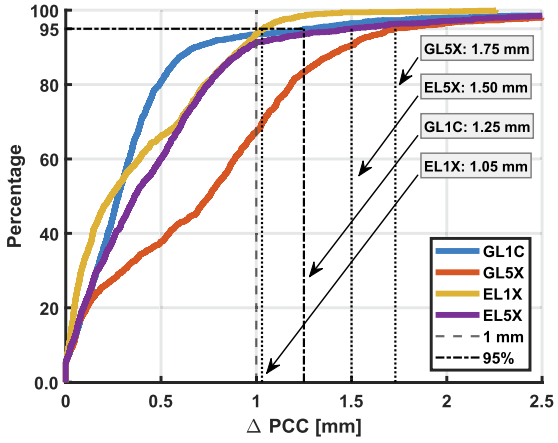

(b)

Fig. 9. Δ PCC obtained by different calibrations of the same antenna (LEIAR20 LEIM), (a) elevation-dependent Δ PCC, (b) cumulative histogram of absolute Δ PCC for various frequencies/signals.

Table 2
Characteristic values of the cumulative histogram for repeated calibrations of receiver antenna pattern for LEIAR20 LEIM for different signals and frequencies (see Fig. 9(b)).

Frequency	<68.3% [mm]	<95.4% [mm]	<99.7% [mm]
GL1C	0.4	1.3	2.3
GL5X	1.0	1.7	2.3
EL1X	0.5	1.0	2.3
EL5X	0.5	1.5	2.3

than 1.5 mm, which can be explained by the fact that only 12 GPS satellites transmit this rather new frequency, so that fewer observations are available with a standard calibration (see Fig. 10). In addition, Fig. 9(a) reveals that the highest differences are found at low elevation angles, which is due to the zero zenith condition.

Fig. 9(b) shows the cumulative histogram of absolute Δ PCC, where in this case not only the elevation but also variations in azimuth are considered. In addition to

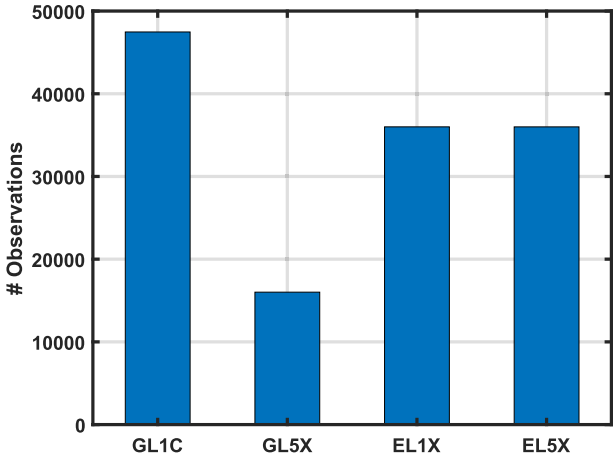

Fig. 10. Total number of observations (dSD) during a standard calibration for the investigated frequencies.

Table 3
RMS and Spread for Δ PCC which have been estimated with Septentrio or Javad receiver for LEIAR25.R3 LEIT.

Frequency	G01	G05	E01	E05
RMS [mm]	0.32	0.20	0.32	0.24
Spread [mm]	0.24	0.60	0.02	0.76

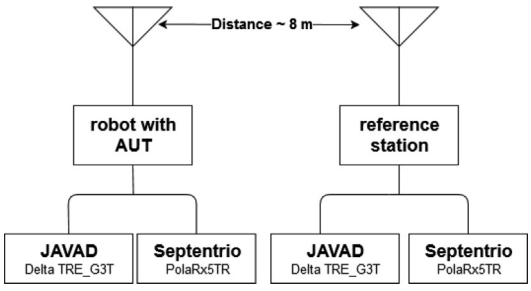

Fig. 11. Sketch of the zero baseline set-up at IfE to analyse the impact of the used receiver on the resulting PCC.

Fig. 9(b), Table 2 lists some characteristic values. From the table and diagram it is quite obvious that for GPS L1C (Galileo EL1X and EL5X) 64% of the differences are below 0.4 mm (0.5 mm). The high difference to GPS L5X (1.0 mm, see Fig. 9(b)) is again mainly due to the significantly reduced number of satellites transmitting this signal. This aspect must be taken into special consideration when analysing the repeatability of the results.

5.2. Repeatability with different receivers

During the calibration of the antennas, geodetic receivers are used to log raw GNSS data. As the combination of antenna and receiver affects the PNT results, receivers of different brands have been used in a zero baseline configuration for the calibration in order to analyse their impact on the estimated PCC (see Fig. 11). Fig. 12 shows the difference patterns between the Javad Delta TRE_3GT and

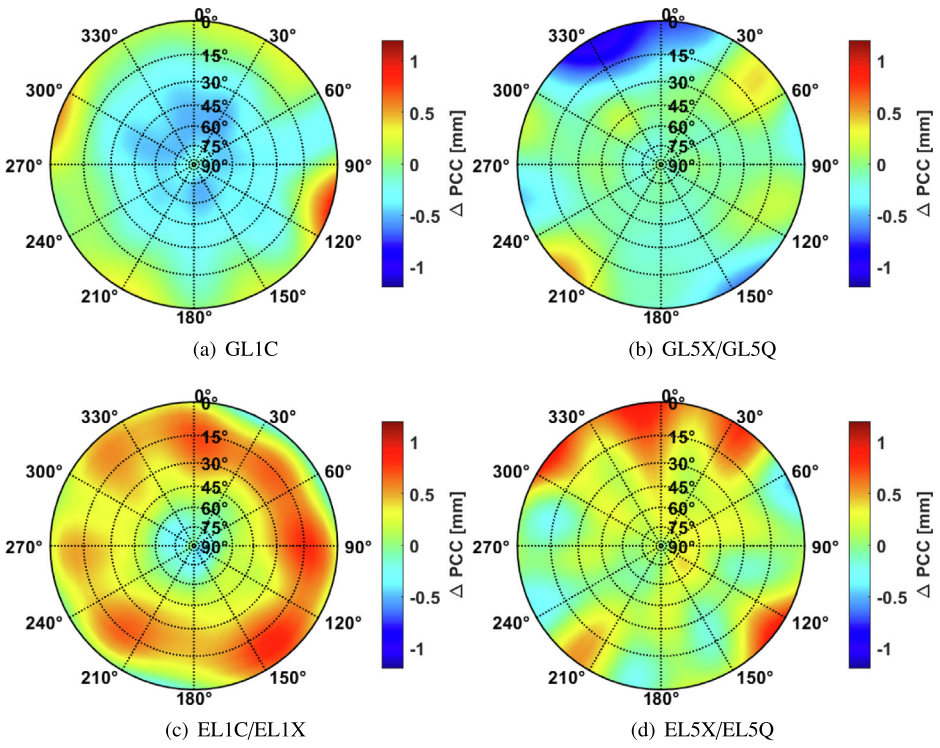

(a) GL1C (b) GL5X/GL5Q

(c) EL1C/EL1X (d) EL5X/EL5Q

Fig. 12. Difference pattern between estimated PCC using Javad Delta TRE_G3T or Septentrio PolaRx5TR receivers for LEIAR25.R3 LEIT on DOY239.

Septentrio PolaRx5TR receiver for LEIAR20 LEIM. Note that Septentrio uses 5Q and Javad 5X as tracking algorithm. It can be seen, that differences up to ±1.2 mm for all four investigated frequencies occur. Table 3 summarises the differences in terms of the RMS of the Δ PCC as well as the datum independent spread. The RMS is less than 0.35 mm and Δs is maximum 0.76 mm.

Fig. 13 underlines the differences between calibrations with different receivers. Elevation-dependent ΔPCC for GL1C, GL5X, EL1X and EL5X are summarized in Fig. 13(a). Due to the zero zenith restriction, the largest PCC differences occur at low elevations. Furthermore, Fig. 13(b) shows that for the L5 frequencies smaller Δ PCC are present, although different tracking algorithms are applied to these frequencies (e.g. GL5Q for Septentrio, GL5X for Javad receivers). Nevertheless, a frequency dependency can be observed, since the elevation-dependent Δ PCC of GL1C and EL1X show a similar behaviour. The same is visible for GL5X and EL5X.

Fig. 13(b) shows the cumulative histogram of absolute Δ PCC values estimated with different receivers. In this case azimuthal and elevation-dependent PCC are considered. There is evidence that almost all Δ PCC are less than 1 mm. The black dotted line indicates a level of 95%, so it is obvious that for all frequencies 95% of the differences are equal or less than 0.65 mm.

6. Validation of estimated PCC

The independent validation of PCC patterns is complicated (Kallio et al., 2018), since by definition GNSS are only one-way ranging systems and therefore no absolute range can be obtained but only pseudo-ranges or relative measurements. In the following subsections, we validate our calibration result using a short baseline common-clock approach. We analyse how the variations of the SD can be explained by the PCC patterns in the observation domain. In addition, we validate different PCC patterns in the coordinate domain in relative positioning mode using well controlled reference coordinates. For both cases we select antennas with different PCC patterns so that the patterns are not eliminated already by single or double differencing.

6.1. Controlled validation setup

A practical experiment was carried out at IfE in order to validate PCC patterns of different institutions in the observation domain. Fig. 14(a) presents the surrounding of the geodetic pillars equipped with the used broadband GNSS antennas – in the foreground a NOV703GGG.R2 NONE on MSD5 and in the background a LEIAR25.R3 LEIT on MSD6. Both pillars have a distance of 7.504 m. Precise coordinates were determined 2018 with sub millimetre accuracy in a local GPS/GLONASS L1 network solution. Terrestrial measurements by total station and precision levelling confirm theses coordinate differences between the geodetic pillars at the level of 0.3–0.4 mm.

The receivers at both stations (Javad Delta TRE_G3T) have been linked to a common external frequency standard. This constellation provides a common-clock short baseline setup. The GNSS measurements were carried out

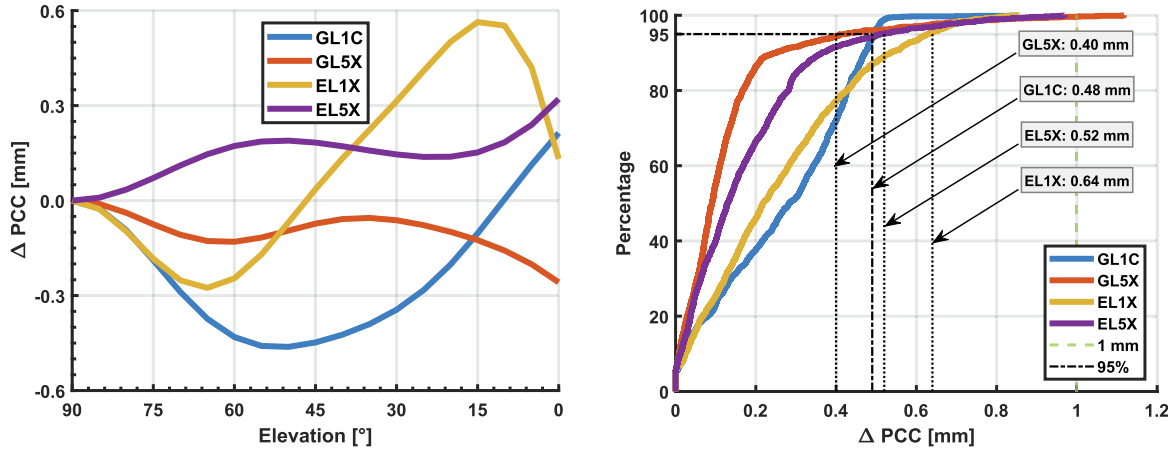

(a) (b)

Fig. 13. Impact of different receivers on the estimated LEIAR25.R3 LEIT PCC, (a) elevation-dependent Δ PCC, (b) cumulative histogram of absolute Δ PCC for various frequencies/signals.

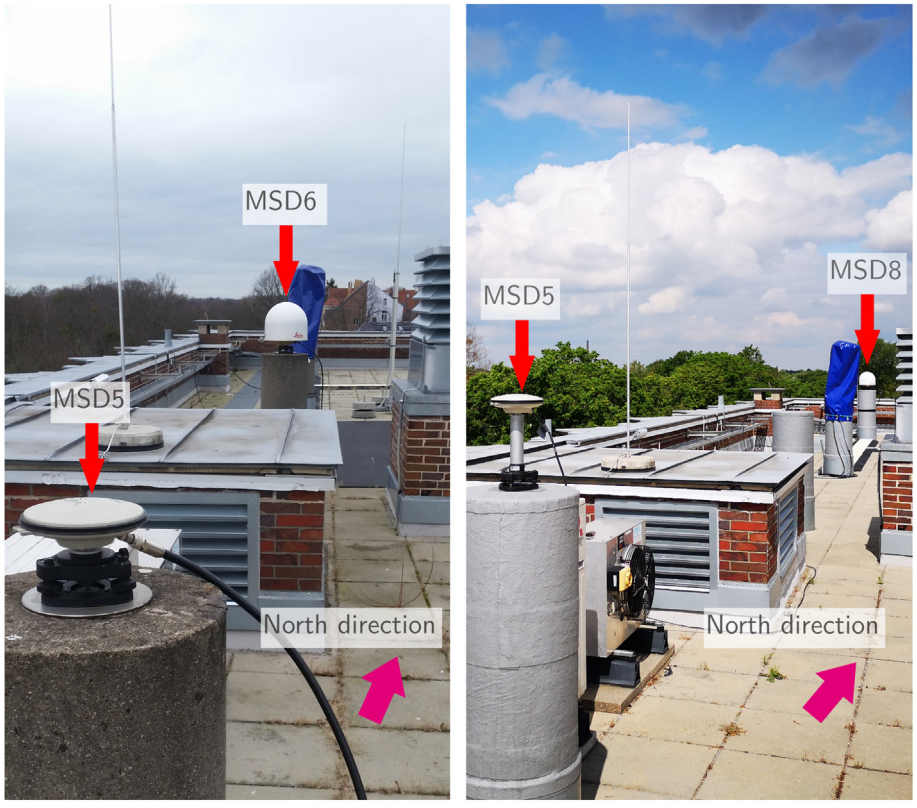

(a) (b)

Fig. 14. Measurement setup at IfE. The labelled antennas are used for a short baseline, common clock experiment to validate estimated PCC in the observation domain (a) and in the coordinate domain (b).

Table 4
Experimental setup for validations in the observation as well as in the coordinate domain. Both times, a NOV703GGG.R2 NONE and a LEIAR25.R3 LEIT antenna are used on the geodetic pillars.

Validation strategy	Baseline length [m]	Geodetic pillars	Used receivers	Data rate
Observation domain	7.504	MSD5 – MSD6	Javad Delta TRE_G3T	1 s
Coordinate domain	20.643	MSD5 – MSD8	Septentrio POLARX5TR	15 s

from February 8th (DOY 039) to 11th (DOY 042) in 2019 with a data rate of 1 Hz.

The experiment to validate PCC patterns in the coordinate domain was carried out from June 10th (DOY 162) to 21st (DOY 173) in 2020 based on 15 sec data sampling using the same type of antennas. Here, the geodetic pillars MSD5 and MSD8 are used, see Fig. 14(b). In order to strongly separate the NOV703GG.R2 rover antenna from the station surrounding, an adapter with a height of approximately 16 cm is used. At both stations Septentrio

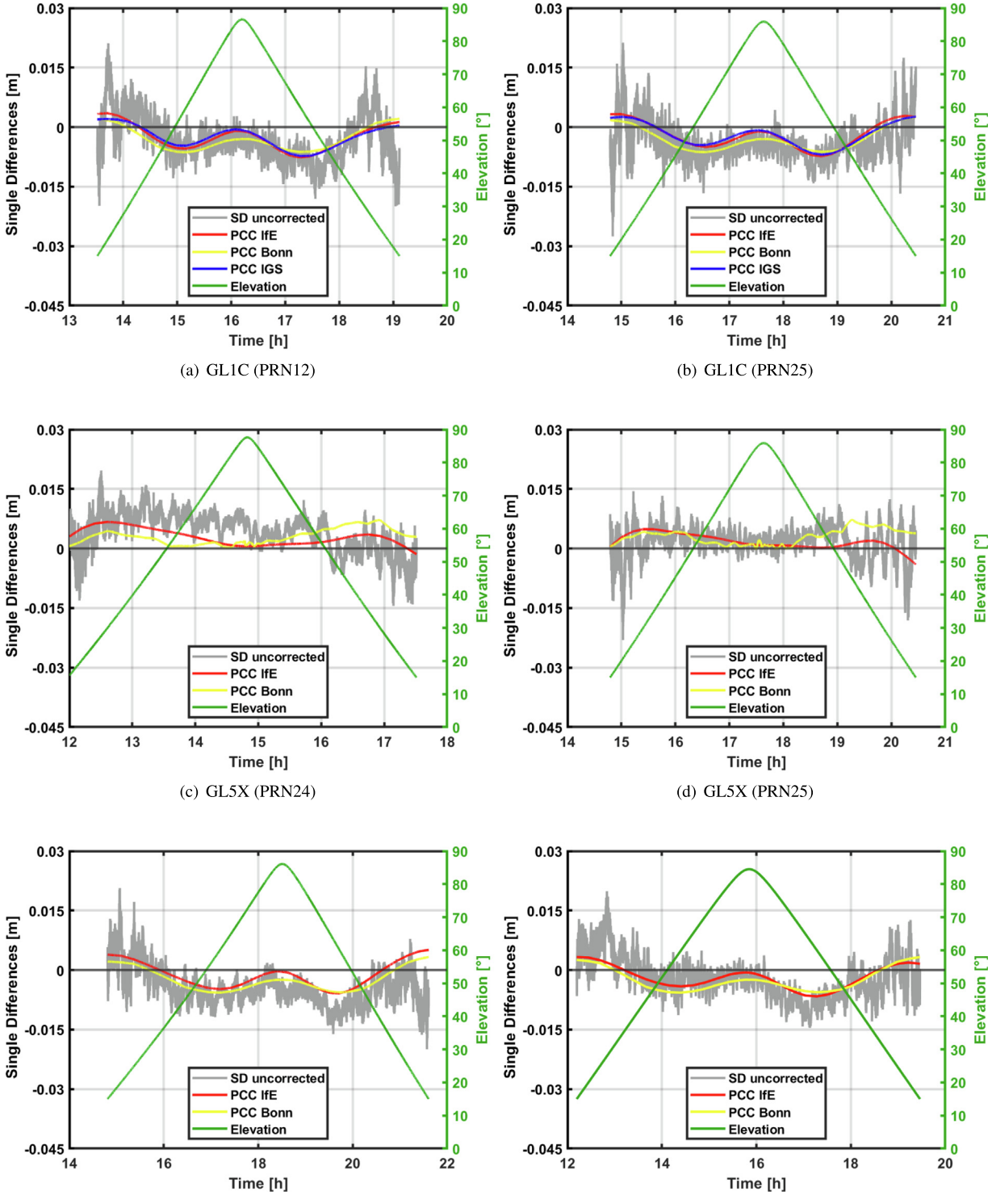

(a) GL1C (PRN12)

(b) GL1C (PRN25)

(c) GL5X (PRN24)

(d) GL5X (PRN25)

(e) EL1X (PRN02)

(f) EL1X (PRN25)

Fig. 15. Comparison of GNSS single differences (SD) on a short baseline with common clock w.r.t. patterns of different approaches (IfE, University Bonn and Geo++). Here, patterns of the used NOV703GGG.R2 and LEIAR25.R3 LEIT are evaluated.

POLARX5TR receivers are linked to an external frequency standard so that again a common-clock short baseline setup with a baseline length of 20.643 m is provided. Table 4 summarises the experimental setups for both validation strategies.

6.2. Validation in the observation domain

To validate the PCC in the observation domain, receiver-to-receiver SD are calculated with respect to the reference coordinates. They contain the difference of the PCC but also the phase ambiguity and a constant initial differential receiver clock error. To avoid big drifts of the SD time series that complicates the comparison of different PCC, an arbitrary height offset d was applied to the observations of all frequencies. It is chosen as the mean PCO_{Up} of G01 and G02 of the respective antennas; here $d = 58.27$ mm for NOV703GGG.R2 and $d = 160.63$ mm for LEIAR25.R3. An integer SD ambiguity N_k has been individually subtracted from each satellite arc k with λ denoting the wavelength of the respective signal

$$N_k = \mathrm{round}(\mathrm{median}(SD_k)/\lambda) \cdot \lambda. \quad (13)$$

Since the SD are not zero mean distributed due to a constant differential receiver clock error between the two stations, a constant part (median) of all SD has been removed. Fig. 15 presents the obtained SD in grey for DOY040 for selected GPS and Galileo satellites. An elevation mask of 15° has been applied to the observations in order to strongly reduce multipath effects due to the challenging surroundings.

The PCC estimated at IfE (red) are compared and validated with chamber calibration results from University Bonn (yellow) available from the European Permanent GNSS Network (EPN) and field calibrations from the IGS, published in the official ANTEX file (blue). Since there are no chamber calibrations available for NOV703GGG.R2, the PCC of LEIAX1202GG are used instead, which has a similar antenna design. Although the ANTEX file to be used for repro3 can be downloaded on the IGS website, these PCC are not taken into account in this validation, since neither Galileo corrections for NOV703GGG.R2 nor a comparable antenna are provided. Since all methods can only determine the shape but not the absolute value of the PCC (remember the unsolved constant part r in Eq. (1)), all PCC patterns are shifted by a common offset best fitting the ensemble of the SD time series.

It can be seen, that the PCC of IfE and PCC of IGS show a good agreement and fit well the SD. Moreover, small differences between the PCC of IfE and PCC of University Bonn can be observed, especially for GL5X and EL1X. This can be explained on the one hand by the different handling of the datum definition (IfE uses zero zenith constraint, University Bonn probably a zero mean constraint) and on the other hand by the use of a slightly different antenna type (LEIAX1202GG instead of NOV703GGG.R2) for PCC of University Bonn.

Table 5 summarizes the mean and maximal improvements in terms of standard deviation σ if IfE PCC are taken into account. The best improvement is present for GL1C. Comparable improvements can be seen for GL5X and EL5X. Furthermore, a reduction of the mean value of the standard deviation by up to 2.6 mm for GL1C (77%) and EL1X (35%) can be reached. If IGS or University Bonn PCC are applied, the mean standard deviation can be reduced to a similar order of magnitude.

Table 5
Mean and maximal improvements of SD in terms of standard deviation σ if IfE PCC are taken into account.

Frequency	$\varnothing\sigma$	max. σ
GL1C	+11%	+ 37%
GL5X	+0%	+ 9%
EL1X	+8%	+ 27%
EL5X	+3%	+ 15%

6.3. Validation in the coordinate domain

The impact of the PCC patterns on the parameters was evaluated for GPS and Galileo using the Bernese GNSS Software (Dach et al., 2015) with consistent multi-GNSS products (Dach et al., 2018). We computed the topocentric coordinate differences of the short baseline when applying different PCC patterns from chamber and robot, see Table 6. Individual daily batches are combined at the normal equation level. For each frequency and linear combination the whole processing was repeated independently. An approximate number of 100 000 observations were used for G L1, G L2, G L0, G L0 + T and GE L1/L5, 1 136 713 for E L1 and E L1/L5 and 1 227 667 for GE L1.

The GPS solutions with troposphere estimates (L1+T, L2+T, L0+T) are processed using a parameter spacing of

Table 6
Summary of tested PCC patterns obtained with different calibration methods.

ID	Method	Remarks
IFE1	robot	IfE, individual, operational robot calibration (Wübbena et al., 2000)
IFE2	robot	IfE, individual, new method (Kröger et al., 2019)
IGS1	robot	IGS (GPS week 2101), type mean (IGS, 2019b)
BONN	chamber	University Bonn, type mean, assuming LEIAX1202 pattern identical with that of NOV703GGG.R2 (EPN, 2019)
IGS2	robot	IGS-R3 (GPS week 2077), type mean for IGS Repo3 (IGS, 2019a), only different values for the Leica AR25, values NOV703GGG.R2 identical with IGS1

1 h for site specific troposphere estimates of station MSD5 only. The Global Mapping function (GMF; Böhm et al. (2006),Böhm et al. (2006)) is applied.

Fig. 16 presents the resulting topocentric coordinate differences to the reference coordinates, when applying different patterns. For all single frequency solution, e.g. GPS

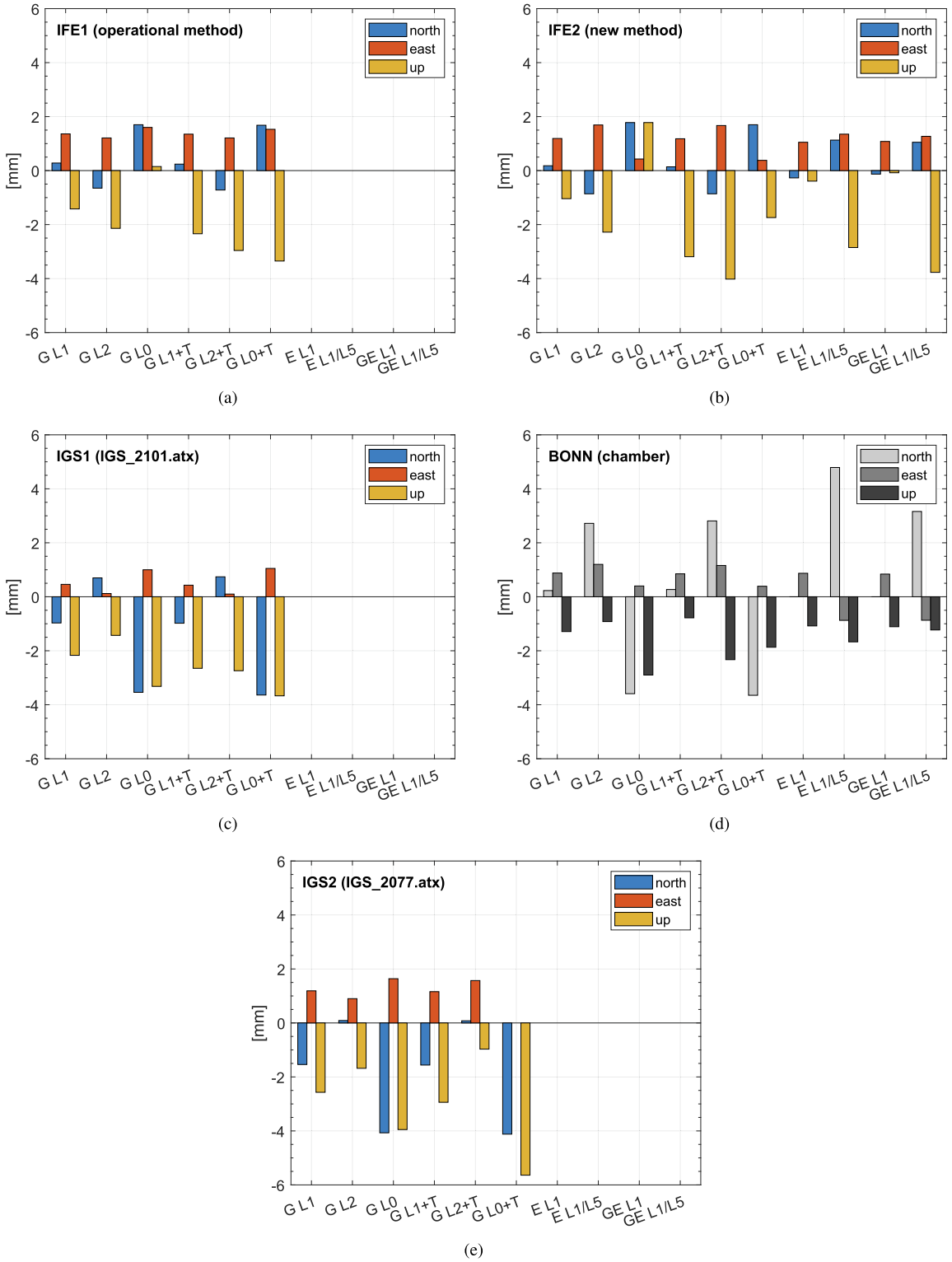

Fig. 16. Topocentric position deviations w.r.t. ground truth when applying several PCC patterns, (a) IFE1 as the operational solution from a typical robot calibration, (b) IFE2, the new multi-GNSS method, (c) the current IGS type mean, (d) BONN as chamber obtained type means, and (e) IGS2 as the IGS-R3 type mean PCC set containing frequency dependent PCC.

GL1, GL2, Galileo EL1, as well as a combined GEL1 analysis, similar deviations to the reference solution below the 3 mm level are obtained. When forming the ionosphere-free linear combination (GL0) of GL1 and GL2, the deviations are changed accordingly to the coefficients of the ionosphere-free linear combination (roughly 2.54 and −1.54 for GPS L1 and L2, respectively). For the IGS patterns this leads to an amplification of the deviation.

The parameter estimation including Zenith Wet Delays (ZWD) increases the height deviations up to 4–6 mm while the horizontal coordinate components stay unchanged, see solutions named L1+T, L2+T, L0+T. This is partially an apparent height shift in the relation of 1:-3 between ZWD and height due to the high correlation between station height and troposphere estimates, although physically no tropospheric delay is present in the double difference observations of the short baseline (Schön et al., 2016; Krawinkel et al., 2014). In addition, these increased deviations can reflect unmodelled station specific effects, like multipath, near field effects, or potential deficiencies of the PCC patterns, (Dilssner et al., 2008; Kersten and Schön, 2016). It is worth noting that the solution with chamber calibrations from University Bonn should be interpreted with care since no calibration values for the NOV703GGG.R2 antenna are available and we used the pattern from Leica AX1202 instead, which has also a pin-wheel antenna design.

7. Conclusion

In this paper, we presented our current strategy for absolute multi-frequency multi-GNSS PCC receiver antenna calibration with a robot in the field. Using three antennas that are widely used in the GNSS community as examples, we have shown that the approach at IfE can achieve absolute PCC for various signals, including the frequencies of GPS L5 and Galileo.

In order to evaluate the approach, a first comparison at the pattern-level is performed. We present a good repeatability of the estimated PCC since the elevation-dependent patterns agree better than 1 mm except for GL5X. Larger differences for this frequency can be explained by less transmitting satellites. The repeatability could be improved, if the same robot movements and same calibration times (taking sidereal satellite geometry repeatability into account) were used. The calibration results also suggest system specific deviations for the L1 to E1 and L5 to E5 patterns, respectively, at the max. 4 mm level. These differences are larger than the impact of different receivers (max. 1.2 mm) but within the repeatability of the estimated PCC (<2.5 mm). However, further confirmation is needed.

A second evaluation was performed at the observation domain for single differences on a short baseline with different antennas. The receivers were connected to the same atomic frequency reference. The corrections show a good agreement following the mean curve of the measured single differences. For GPS L1, with IfE and IGS PCC almost similar results were obtained.

A third evaluation was carried out in the coordinate domain, estimating topocentric coordinate differences with various PCC sets and for several linear combinations. We showed that for L1 and E1 as well as the combination of these frequencies, all coordinate solutions are quite similar and result in high accuracy. The differences of our new solution to the reference are for most frequencies below 1 mm for horizontal and less than 2.2 mm for the height component when using different antenna types at the two endpoints of the short baseline. The deviation for ionosphere-free linear combinations changes according to the coefficients used for computing the respective linear combinations. Finally, the estimation of tropospheric zenith wet delays leads to apparent height shifts for all applied PCC due to the high correlation between height and tropospheric parameters. Consequently, all estimated parameters (including tropospheric delays) have to be analysed when comparing the impact of different PCC on the estimated parameters.

Data availability

The PCC estimated with the newly developed multi-frequency multi-GNSS calibration process at IfE are freely accessible in ANTEX format for further comparisons and evaluations under the doi https://doi.org/10.25835/0075279 (Kröger et al., 2019).

Declaration of Competing Interest

The authors declare that they have no known competing financial interests or personal relationships that could have appeared to influence the work reported in this paper.

Acknowledgement

We thank the anonymous reviewers for their hints, valuable remarks and discussions that improved the manuscript.

References

Altamimi, Z., Rebischung, P., Métivier, L., Collilieux, X., 2016. ITRF2014: A new release of the International Terrestrial Reference Frame modelling nonlinear station motions. J. Geophys. Res. 121, 6109–6131. https://doi.org/10.1002/2016JB013098.

Becker, M., Zeimetz, P., Schönemann, E., 2010. Anechoic Chamber calibrations of phase center variations for new and existing GNSS signals and potential impacts in IGS processing. In: Presentation at the IGS Workshop 2010 and Vertical Rates Symposium, June 28 - July 2, Newcastle upon Tyne, United Kingdom of Great Britain. ftp://www.ngs.noaa.gov/pub/abilich/calibPapers/.

Beer, S., Wanninger, L., Heßelbarth, A., 2019. Galileo and GLONASS group delay variations. GPS Solut. 24. https://doi.org/10.1007/s10291-019-0939-7.

Böhm, J., Niell, A., Tregoning, P., Schuh, H., 2006. Global mapping function (GMF): A new empirical mapping function based on

numerical weather model data. Geophys. Res. Lett. 33, L07304. https://doi.org/10.1029/2005GL025546.

Bilich, A., Mader, G., Geoghegan, C., 2018. 6-axis robot for absolute antenna calibration at the US National Geodetic Survey. In: Presentation at the IGS Workshop 2018, October 29 - November 2, Wuhan, China. Poster.

Böder, V., Menge, F., Seeber, G., Wübbena, G., Schmitz, M., 2001. How to Deal With Station Dependent Errors, New Developments of the Absolute Field Calibration of PCV and Phase-Multipath With a Precise Robot. In: Proceedings of the 14th International Technical Meeting of the Satellite Division of The Institute of Navigation (ION GPS 2001), September 11–14. Institute of Navigation (ION) IEEE, Salt Lake City, UT, USA, pp. 2166–2176.

Breva, Y., Kröger, J., Kersten, T., Schön, S., 2019. Estimation and validation of receiver antenna codephase variations for multi GNSS. In: 7th International Colloquium on Scientific and Fundamental Aspects of GNSS, September 4–6, Zürich, Switzerland.

Bruyninx, C., Legrand, J., 2017. Receiver Antenna Calibrations Available from the EPN CB. In: EUREF AC Workshop, October 25–26, Brussels, Belgium. URL http://www.epncb.oma.be/_newseventslinks/workshops/EPNLACWS_2017/pdf/02_EPN_Combination/03_Bruyninx_Calibrations.pdf.

Caizzone, S., Circiu, M.-S., Elmarissi, W., Enneking, C., Felux, M., Yinusa, K., 2019. Antenna influence on global navigation satellite system pseudorange performance for future aeronautics multifrequency standardization. Navigation 66, 99–116. https://doi.org/10.1002/navi.281.

Dach, R., Lutz, S., Walser, P., Fridez, P. (Eds.), 2015. Bernese GNSS Software Version 5.2. University of Bern, Bern Open Publishing. Doi: 10.7892/boris.72297.

Dach, R., Schaer, S., Arnold, D., Kalarus, M.S., Prange, L., Stebler, P., Villiger, A., Jäggi, A., 2018. CODE final product series for the IGS. doi: 10.7892/BORIS.75876.3.

DeMets, C., Gordon, R.G., Argus, D.F., 2010. Geologically current plate motions. Geophys. J. Int. 181, 1–80. https://doi.org/10.1111/j.1365-246x.2009.04491.x.

Dilssner, F., Seeber, G., Wübbena, G., Schmitz, M., 2008. Impact of near-field effects on the gnss position solution. In: Proceedings of the 21st International Technical Meeting of the Satellite Division of the Institute of Navigation (ION GNSS 2008), pp. 612–624.

EPN, 2019. European Permanent Network FTP Server. ftp://epncb.eu/pub/station/general/.

Garbin, E., Defraigne, P., Krystek, P., Piriz, R., Bertrand, B., Waller, P., 2018. Absolute calibration of GNSS timing stations and its applicability to real signals. Metrologia 56, 015010. https://doi.org/10.1088/1681-7575/aaf2bc.

Görres, B., Campbell, J., Becker, M., Siemes, M., 2006. Absolute calibration of GPS antennas: laboratory results and comparison with field and robot techniques. GPS Solut. 10, 136–145. https://doi.org/10.1007/s10291-005-0015-3.

Hu, Z., Zhao, Q., Chen, G., Wang, G., Dai, Z., Li, T., 2015. First Results of Field Absolute Calibration of the GPS Receiver Antenna at Wuhan University. Sensors 15, 28717–28731. https://doi.org/10.3390/s151128717.

IGS, 2015. RINEX - The Receiver Independent Exchange Format Version 3.03. Technical Report. URL https://kb.igs.org/hc/article_attachments/202583897/RINEX303.pdf.

IGS, 2019a. Conventions and modeling for repo3. URL: http://acc.igs.org/repro3/repro3.html (29.01.2020).

IGS, 2019b. International GNSS Service FTP Server. URL: https://files.igs.org/pub/station/general.

Johnston, G., Riddell, A., Hausler, G., 2017. In: Montenbruck, O., Teunissen, P. (Eds.), Springer Handbook of Global Navigation Satellite Systems. The International GNSS Service. Springer International Publishing, pp. 967–982. doi:10.1007/978-3-319-42928-1_33 (Chapter 33).

Kallio, U., Koivula, H., Lahtinen, S., Nikkonen, V., Poutanen, M., 2018. Validating and comparing GNSS antenna calibrations. J. Geodesy 93, 1–18. https://doi.org/10.1007/s00190-018-1134-2.

Kersten, T., 2014. Bestimmung von Codephasen-Variationen bei GNSS-Empfangsantennen und deren Einfluss auf die Positionierung, Navigation und Zeitübertragung (Determination of Codephase Variations for GNSS Receiving Antennas and Their Impact on Positioning, Navigation and Timing). Ph.D. thesis Deutsche Geodätische Kommission (DGK) bei der Bayerischen Akademie der Wissenschaften (BADW), No. 740. doi:10.15488/4003.

Kersten, T., Schön, S., 2017. GPS code phase variations (CPV) for GNSS receiver antennas and their effect on geodetic parameters and ambiguity resolution. J. Geodesy 91, 579–596. https://doi.org/10.1007/s00190-016-0984-8.

Kersten, T., Schön, S., 2010. Towards modeling phase center variations for multi-frequency and multi-GNSS. In: 2010 5th ESA Workshop on Satellite Navigation Technologies and European Workshop on GNSS Signals and Signal Processing (NAVITEC). IEEE, pp. 1–8. https://doi.org/10.1109/navitec.2010.5708040.

Kersten, T., Schön, S., 2016. Receiver Antenna Phase Center Models and Their Impact on Geodetic Parameters. In: Rizos, C. (Ed.), Proceedings of the IAG General Assembly 2015. International Association of Geodesy Symposia. https://doi.org/10.1007/1345_2016_233.

Krawinkel, T., Lindenthal, N., Schön, S., 2014. Scheinbare Koordinatenänderungen von GPS-Referenzstationen: Einfluss von Auswertestrategien und Antennenwechseln (Apparent Coordinate Changes of GPS Reference Stations: Impact of Processing Strategies and Antenna Changes). ZfV 139, 252–263.

Kreemer, C., Blewitt, G., Klein, E.C., 2014. A geodetic plate motion and global strain rate model. Geochem. Geophys. Geosyst. 15, 3849–3889. https://doi.org/10.1002/2014gc005407.

Kröger, J., Breva, Y., Kersten, T., Schön, S., 2019. Robot based phase centre corrections for new GNSS signals. doi: 10.25835/0075279 resource: IfE20_2132.zip.

Kröger, J., Breva, Y., Kersten, T., Schön, S., 2019. Phase Center Corrections for new GNSS-Signals. In: Geophysical Research Abstracts 21 number 21 in Geophysical Research Abstracts. doi: 10.15488/4682.

Mader, G., Bilich, A., Geoghegan, C., 2012. Absolute GNSS Antenna Calibration at the National Geodetic Survey. In: Presentation at the European Geophysical Union General Assembly 2012, vol, 14. Geophysical Research Abstracts #EGU2012-3080. Poster, URL: http://meetingorganizer.copernicus.org/EGU2012/EGU2012-3080.pdf (30.01.2020).

Menge, F., Seeber, G., Völksen, C., Wübbena, G., Schmitz, M., 1998. Results of the absolute field calibration of GPS antenna PCV. In: Proceedings of the 11th International Technical Meeting of the Satellite Division of The Institute of Navigation (ION GPS 1998), September 15–18. Institute of Navigation IEEE, Nashville, TN, USA, pp. 31–38.

Rao, B.R., Kunysz, W., Fante, R.L., McDonals, K., 2013. GPS/GNSS Antennas. Artech House Publishers, Norwood, USA.

Rothacher, M., Schaer, S., Mervat, L., Beutler, G., 1995. Determination of Antenna Phase Center Variations using GPS Data. In: Presentation at the IGS Workshop - Special Topics and new Directions, May 15–18, Potsdam, Germany, p. 16.

Rothacher, M., Schmid, R., 2010. ANTEX: The Antenna Exchange Format, Version 1.4. Technical Report.

Schmolke, A., Wanninger, L., Frevert, V., 2015. Erste GNSS-Antennenkalibrierungen im Feldverfahren auf neuen Signalfrequenzen (First GNSS antenna calibrations in the field for new frequencies). zfv – Zeitschrift für Geodäsie. Geoinformation und Landmanagement 140, 283–289.

Schön, S., 2007. Affine distortion of small gps networks with large height differences. GPS Solut. 11. https://doi.org/10.1007/s10291-006-0042-8.

Schön, S., Kersten, T., 2013. On adequate Comparison of Antenna Phase Center Variations. In: Presentation at the American Geophysical Union, Annual Fall Meeting 2013, December 09.-13., San Francisco, CA, USA Geophysical Abstracts #G13B-0950.

Schön, S., Pham, H., Krawinkel, T., 2016. On removing discrepancies between local ties and gps-based coordinates. In: Presentation at the International Symposium on Earth and Environmental Sciences for Future Generations. Springer, pp. 245–252.

Stutzman, W., 2013. Antenna theory and design, third ed. Wiley, Hoboken, NJ.

Villiger, A., Prange, L., Dach, R., Zimmermann, F., Kuhlmann, H., Jäggi, A., 2019. GNSS scale determination using chamber calibrated ground and space antenna pattern. Geophys. Res. Abstracts 21. https://doi.org/10.7892/BORIS.130383.

Villiger, A., Prange, L., Dach, R., Zimmermann, F., Kulmann, H., Jäggi, A., 2018. Consistency of antenna products in the MGEX environment. International GNSS Service. https://doi.org/10.7892/BORIS.121335.

Wanninger, L., Sumaya, H., Beer, S., 2017. Group delay variations of GPS transmitting and receiving antennas. J. Geodesy 91, 1099–1116. https://doi.org/10.1007/s00190-017-1012-3.

Willi, D., Lutz, S., Brockmann, E., Rothacher, M., 2019. Absolute field calibration for multi-GNSS receiver antennas at ETH zurich. GPS Solut. 24. https://doi.org/10.1007/s10291-019-0941-0.

Wu, J., Wu, S., Hajj, G., Bertiger, W., Lichten, S., 1993. Effects of antenna orientation on GPS carrier phase. Manuscripta geodaetica 18, 91–98, http://www.mendeley.com/research/effects-of-antenna-orientation-on-gps-carrier-phase/.

Wübbena, G., Schmitz, M., Menge, F., Böder, V., Seeber, G., 2000. Automated Absolute Field Calibration of GPS Antennas in Real-Time. In: Proceedings of the 13th International Technical Meeting of the Satellite Division of The Institute of Navigation (ION GPS 2000), September 19-22. Institute of Navigation (ION), Salt Lake City, UT, USA, pp. 2512–2522.

Wübbena, G., Schmitz, M., Warneke, A., 2019. Geo++ Absolute Multi Frequency GNSS Antenna Calibration. In Presentation at the EUREF Analysis Center (AC) Workshop, October 16–17, Warsaw, Poland. URL: http://www.geopp.com/pdf/gpp_cal125_euref19_p.pdf (29.01.2020).

Zeimetz, P., 2010. Zur Entwicklung und Bewertung der absoluten GNSS-Antennenkalibrierung im HF-Labor (On further improvements and the validation of the absolute GNSS-antenna calibration in HF-laboratories). Ph.D. thesis Institut für Geodäsie und Geoinformation, Universität Bonn. URL http://hdl.handle.net/20.500.11811/1409.